Partitioning Sequences and Arrays of Directional Ocean Wave Spectra into Component Wave Systems

THOMAS W. GERLING

The Johns Hopkins University, Applied Physics Laboratory, Laurel, Maryland

(Manuscript received 8 April 1991, in final form 8 October 1991)

ABSTRACT

A method for characterizing wave systems from temporal sequences and spatial arrays of directional ocean surface gravity-wave spectral estimates is presented. The method is structured in two major stages. In the first data-intensive stage, individual spectra are parameterized in terms of the directions, periods, and significant wave heights of wave systems represented in that spectrum. In the second stage, wave systems from spectra are associated with similar wave systems in neighboring spectra, and "large-scale wave systems" representing activity occurring continuously over groups of contiguous spectra are determined. This high-level description of the ocean surface wave field represents a considerable data reduction that preserves directional information in a more meaningful way than either average wave directions computed over the entire spectrum or wind sea-swell decompositions. Each large-scale wave system is normally caused by a distinct meteorological event. Data from the Labrador Sea Extreme Waves Experiment (LEWEX) are used to illustrate applications to numerical wave model and buoy spectra, and these methods should be useful in other spectral data comparison experiments. Other potential applications include the interpretation and archival of global wave-model analyses and the compression of wave spectra in a manner sufficient to preserve information necessary for numerical wave model data-assimilation schemes.

1. Introduction

Large datasets consisting of arrays of directional ocean wave spectral estimates are increasingly important for scientific and operational activities. Various numerical wind-wave models produce forecasts and analyses of directional wave spectra on global scales (The WAMDI Group 1988; Clancy et al. 1986). Directional buoys produce datasets extending sometimes for years with a several-hour sampling interval (Audenson et al. 1982; Allender et al. 1989). Anticipated satellite systems will produce a dense sampling of directional wave spectral estimates (Gerling and Beal 1991). It is desirable to be able to characterize the variability in these datasets in such a way that their directional aspects can be appreciated. When the dataset consists of just a few observations, it is practical to view all of the directional spectra. However, when applying this approach to large datasets consisting of hundreds or perhaps even thousands of spectra, one can loose sight of the large-scale variability due to the very large amount of information. In a complicated comparison experiment, such as the one that motivated this work, differences between data sources might be difficult to characterize through point-by-point comparisons of individual wave spectra (Gerling 1991). To properly characterize some differences it is necessary to also consider observations that are spatially or temporally displaced. Possibly the only practical way of accomplishing this with large datasets of directional spectra is to calculate reduced parameters and through them obtain a sense of the variability. For global wave model datasets it is common to calculate an average wave height and direction from each spectrum, or perhaps a vector for the wind sea component of the spectrum and another for the swell component (see, for example, The WAMDI Group 1988; Figs. 28, 29, 30, 33). For other datasets, such as those from directional buoys or future remotely sensed spectra, it is possible to do the same. However, important aspects of ocean wave variability can be missed by these statistics, since spectral information due to generating sources separated in space and time is averaged in the calculation of average wave height and direction. Even wind sea-swell separation schemes might represent too much averaging, since the swell component might consist of multiple wave systems. For this reason, a new data reduction method has been developed that characterizes individual, potentially multimodal spectra in terms of component wave systems and determines larger-scale spatiotemporal patterns of wave activity from this information. These patterns can represent a consid-

Corresponding author address: Dr. Thomas W. Gerling, The Johns Hopkins University, Applied Physics Laboratory, Johns Hopkins Rd., Laurel, MD 20723-6099.

erable data reduction and at the same time be easier to interpret than the average quantities described previously.

The data-reduction methods described in this article are intended to describe wave-field variability as Snodgrass et al. (1966) did, that is, as a superposition of remotely generated wave trains. In that article, the evolution of features present in sequences of frequency spectra was related to source regions of remotely generated waves. Time series from a bottom-mounted pressure sensor were arranged in a two-dimensional format of energy as a function of frequency and time, $E(f, t)$. Remotely generated wave trains corresponded to "ridges" in the graph of this function. The slope of the ridge was related to the distance to the source region, and the zero-frequency intercept was related to the time of generation. Using an array of seven such sensors distributed across the Pacific Ocean, it was possible to estimate the location of the generating regions for the wave trains and track their propagation. In this way, much of the variability seen in the pressure records was accounted for. In contrast, the algorithms described here assume a directional wave spectrum as input rather than a scalar time series of pressure. Directional information can then be obtained from a time series at a single location. Moreover, the algorithms described here operate automatically and also produce an estimate of the variance attributable to each component wave system.

In this article, three algorithms that were developed to help understand the variability contained in large datasets of directional spectra will be discussed and illustrated with time series of directional spectra from LEWEX. Specifically, these are the spectral-partitioning algorithm or SPA (which reduces individual spectra), the pattern-extraction algorithm or PEA (which determines spatial or temporal patterns in the reduced parameters), and finally the pruning algorithm or PA (which selects the appropriate SPA statistics with which to describe wave systems using information from PEA).

2. The spectral-partitioning algorithm

The spectra in this paper are functions $S(f, \theta)$ of frequency and wave propagation direction. Here $S(f, \theta)$ gives a decomposition of the total wave height variance in terms of f and θ:

$$\text{total wave height variance} = \int_{f,\theta} S(f, \theta) f df d\theta.$$

For finite Δf and $\Delta\theta$, $S(f, \theta) f \Delta f \Delta\theta$ gives the amount of the total surface wave height variability accounted for by wave variance in the bin centered at (f, θ) having width $(\Delta f, \Delta\theta)$. The directional buoy discussed in this article, the Wavescan (Allender et al. 1989), observes time series of heave and also east and north slope so that only the first four Fourier coefficients in each frequency band are estimated. From these, an estimate of $S(f, \theta)$ can be constructed, as will be discussed in more detail below.

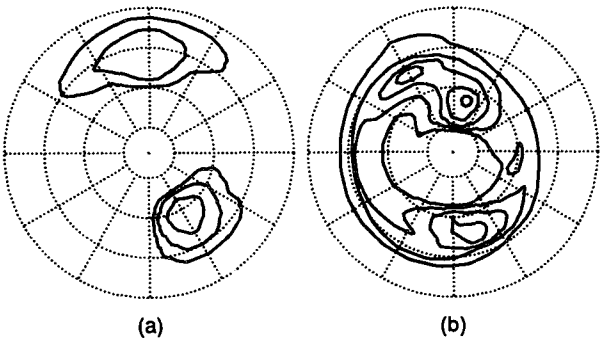

FIG. 1. Two typical multimodal directional wave spectra at one LEWEX experimental site (50°N, 45°W) generated by (a) WAM at 0000 UTC 13 March 1987 and (b) the Wavescan buoy using the maximum entropy method at 2230 UTC 17 March 1987.

The SPA partitions the support of the directional spectrum (the region over which the spectrum assumes nonzero values) into regions that are attributable to component wave systems. The spectral signature of each wave system is then characterized with a small number of descriptive parameters, such as peak frequency and direction, average frequency and direction, and associated variance.

The SPA can be understood as generalizing a partitioning scheme that could be used in an obvious situation, such as that depicted in Fig. 1a, which shows a wave spectrum that is composed of two completely separate portions.[1] In that spectrum, a low-frequency swell portion and also a higher-frequency wind-sea portion can be seen. The obvious partitioning procedure to use here is to treat each portion as though it were a distinct spectrum and calculate the usual univariate statistics on each portion separately. However, another spectrum that defeats this scheme is the wave spectrum depicted in Fig. 1b. This spectrum is trimodal, but does not separate into distinct portions like the

[1] The radial scale for spectra displayed in this article is log frequency, with a range of 0.05–0.2 Hz. Calibration circles corresponding to wavelengths of 400, 200, 100, and 50 m and calculated using the dispersion relation for deep-water gravity waves ($\omega^2 = gk$) are also shown. These calibration circles also correspond to wave periods of approximately 16, 11.5, 8, and 5.5 s. The quantity contoured has units of square meters square seconds ($m^2 s^2$), and the levels of the contours increase geometrically. Each level exceeds the closest lower one by a factor of about 2.12. The spectra indicate the direction toward which waves propagate, although the meteorological convention is used to name wave systems. Thus, a wave system propagating toward the south is usually referred to as a "northerly" wave system. With this format, it is possible to display spectral variance in both the wind sea and swell regions of the spectrum and still display the results in absolute units. However, the visual perception of spectral volume does not correspond to wave height variance [units of square meters (m^2)] because of the log scales used.

simpler spectrum of Fig. 1a. In fact, a band of energy completely surrounds the spectral origin in the spectrum of Fig. 1b. The idea proposed here is to initially assume that all spectral modes (i.e., local peaks) might represent information concerning distinct wave systems. Then, after these initial estimates are available, the significance of each wave system is assessed on the basis of its variance estimate and its spatial or temporal persistence.

The first step in partitioning the wave height variance among the various spectral modes is to determine if the support of the spectrum $S(f, \theta)$ is connected. If so, then determine if a level l exists such that the support of S thresholded at l, S^l, is not connected. The thresholded spectrum S^l is defined as

$$S^l = \begin{cases} S(f, \theta) & \text{if} \quad S(f, \theta) \geq l \\ 0 & \text{if} \quad S(f, \theta) < l. \end{cases}$$

The first case to consider occurs if such an l does not exist. Then the spectrum has only one mode, and its location will be calculated and the candidate wave system will be assigned a strength of 1. These strength estimates are analogous to conditional probabilities and can be converted to variance estimates by multiplying by the total wave height variance.

The second case occurs if such an l exists. Then find the lowest value and call it l_0. To conserve storage space, the spectra have been scaled to lie between 0 and 255 (the range of 1-byte integers) and then rounded to the nearest integer. Therefore, only this discrete set of values is searched for l_0. Express the support of S^{l_0} as the union of a minimal number of connected regions R_{i_0}:

$$\bigcup_{i_0=1}^{n_0} R_{i_0}. \tag{1}$$

For each of these regions calculate a quantity M_{i_0}, which will ultimately be used to estimate the strength of a component wave system recursively:

$$M_{i_0} = \int_{R_{i_0}} S(f, \theta) f df d\theta. \tag{2}$$

Also calculate

$$P_{i_0} = \frac{M_{i_0}}{\sum M_{i_0}}. \tag{3}$$

Now, for each of the regions R_{i_0}, perform the procedure just described: first, determine if a level l exists such that the support of S restricted to R_{i_0} and thresholded at l, $S^l_{R_{i_0}}$, is not connected. The restricted spectrum S_R is defined as

$$S_R = \begin{cases} S(f, \theta) & \text{if} \quad (f, \theta) \in R \\ 0 & \text{if} \quad (f, \theta) \notin R. \end{cases}$$

As before, if no such l exists, then this portion of the spectrum has only one mode, and its location will be calculated and assigned a strength of P_{i_0}. However, if such an l exists, then find the lowest and call it l_{i_0}. Express the support of $S^{l_{i_0}}_{R_{i_0}}$ as the union of a minimal number of connected regions $R_{i_0 i_1}$:

$$\bigcup_{i_1=1}^{n_{i_0}} R_{i_0 i_1}. \tag{4}$$

For each of these regions, calculate as before a quantity $M_{i_0 i_1}$:

$$M_{i_0 i_1} = \int_{R_{i_0 i_1}} S(f, \theta) f df d\theta. \tag{5}$$

Also calculate

$$P_{i_0 i_1} = P_{i_0} \frac{M_{i_0 i_1}}{\sum_{i_1} M_{i_0 i_1}}. \tag{6}$$

The algorithm continues now to consider each of the regions $R_{i_0 i_1}$ and assigns a strength of $P_{i_0 i_1}$ to a unique mode, but if one does not exist, it goes on to calculate $l_{i_0 i_1}$, which in turn determines

$$S^{l_{i_0 i_1}}_{R_{i_0 i_1}},$$

its support

$$\bigcup_{i_2=1}^{n_{i_0 i_1}} R_{i_0 i_1 i_2}, \tag{7}$$

the corresponding strength estimates

$$P_{i_0 i_1 i_2} = P_{i_0 i_1} \frac{M_{i_0 i_1 i_2}}{\sum_{i_2} M_{i_0 i_1 i_2}},$$

and so on. The procedure results in a hierarchically structured description of the spectrum, a "tree structure," that generalizes the conventional statistics of average wave propagation direction and total significant wave height (SWH). These quantities are related to those at the base of the tree, whereas the arborization consists of the location estimates and the recursively calculated strength estimates. It corresponds to a successively finer fractionation of wave height variance among component wave systems. This tree structure lends itself relatively easily to the further processing stages PEA and PA that are discussed later. The PA results in "pruning," or removal of weak or spurious peaks from the description of noisy spectra. If a mode is judged to be insignificant, the corresponding "branch" is "pruned," and the statistics used are the more averaged ones calculated at the previous level. Finally, when the algorithm finishes, a set of weights $P_{i_0 i_1 i_2 \ldots i_n}$ will sum to 1 and are used to partition the wave height variance among the various wave systems represented in the spectrum. Frequency and direction at the local spectral maximum ($f^{\max}$ and $\theta^{\max}$) as well as average frequency and direction (f^{avg} and θ^{avg}) are

computed over each of the regions $R_{i_0 i_1 i_2 \ldots i_n}$. At the beginning of the description of this algorithm, it was supposed that the support of $S(f, \theta)$ was connected. If it is not, an identical procedure is followed, except that the l_0 at the beginning is now 0.

3. Application to LEWEX spectral time series

The Labrador Sea Extreme Waves Experiment (LEWEX) occurred 13–19 March 1987 (Beal 1991) and involved measurements at two locations off Newfoundland. At each location, a research vessel deployed wave measuring buoys; the vessels were the Canadian *Quest* at 50°N, 47.5°W and the Dutch *Tydeman* at 50°N, 45°W. LEWEX was planned to provide comparisons between various numerical wave models, directional buoys, and airborne (some potentially spaceborne) radar remote sensors in a natural environment expected to produce large seas. This expectation, which was based on climatology, unfortunately was not realized, but a rather complex dataset with SWH variation between 2 and 6 m and spectra that were at times trimodal was obtained. SWH is defined in terms of the directional frequency spectrum $S(f, \theta)$ as

$$\text{SWH} = 4\left[\int_{f,\theta} S(f, \theta) f df d\theta\right]^{0.5}.$$

The units of $S(f, \theta)$ are square meters square seconds ($m^2\ s^2$) in this case, although for wavenumber spectra derived from radar imagery, units of meters to the fourth power (m^4) would be more natural. A hindcast wind field covering much of the North Atlantic was constructed by Oceanweather, Inc., (Cardone 1991) and distributed to various modelers in October 1987. A complete description of LEWEX and comparisons among the various spectral observations and models run with this hindcast wind field can be found in the papers contained in Beal (1991). Although nine modeling groups and many wave-measuring devices were involved in LEWEX, only the results from three models run with the hindcast wind field and one directional buoy will be used for illustration in this paper. Each of these data sources has unique aspects useful for gaining a sense of the utility and limitations of the methods discussed here. These data sources are the third-generation WAM (wave model) (The WAMDI Group 1988), the second-generation model VAG (Guillaume 1987, 1991), and the "first-generation" U.S. Navy Global Spectral Ocean Wave Model (GSOWM) (Clancy et al. 1986) for which an archived semiglobal dataset was available. For a discussion of this generational nomenclature and various implementations, see the report by The SWAMP Group (1985).

Data from one heave, pitch, and roll directional buoy, the Wavescan (Krogstad 1987; Allender et al. 1989), will also be discussed. This buoy was moored from 14 March through 18 March at the location of the *Tydeman* and provided a continuous series of heave and also north and east slope observations every 1.5 h. Directional spectral estimates can be constructed from the buoy-measured quantities with any of a variety of methods (Longuet-Higgins et al. 1963; Long and Hasselmann 1979; Oltman-Shay and Guza 1984; Lygre and Krogstad 1986), although sometimes quantities more basic than a directional spectral estimate are computed (Kuik et al. 1988; Guillaume 1990) to avoid possible biases resulting from assumptions implicit to the particular reconstruction method being used. For the work described in this paper, the maximum entropy method (MEM) as described in Lygre and Krogstad (1986) was used to obtain two-dimensional spectral estimates, which were then reduced in the same manner as wave-model spectra. The maximum entropy method in LEWEX produced believable spectral estimates (Gerling 1991), since the same wave systems were seen in both the MEM buoy spectra and the WAM and other model spectra. When differences between buoy spectra and model spectra occurred, they were explainable.

A rather complicated trimodal Wavescan spectrum computed using the maximum entropy method is shown in Fig. 1b. This spectrum will be used to illustrate the three data-reduction algorithms. As noted earlier, this spectrum exhibits three wave systems, although they are not well separated like those in Fig. 1a. Proceeding according to the scheme described in section 2, the spectrum was scaled to occupy the range of 1-byte integers, 0–255. At level 0, the support of the spectrum is connected, but the lowest level l_0 at which the support of the thresholded spectrum S^{l_0} is not connected is 23. The resulting regions R_0 and R_1 specified in (1) are shown in Fig. 2a. The values M_0 and M_1 are computed for these two regions with (2) to give the factors P_0 and P_1 from (3) that will be used to fractionate the total variance V if the decision is made that each region supports a separate wave system. The values calculated for P_I, as well as other descriptive pa-

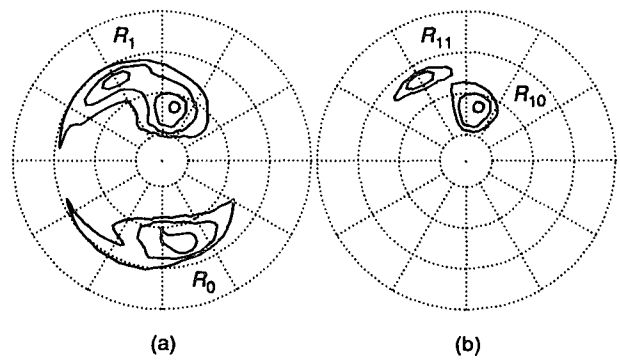

FIG. 2. Contour diagrams for thresholded spectra used in the partitioning of the Wavescan spectrum of Fig. 1b. In (a), the spectrum is thresholded at level 23 (spectra scaled between 0 and 255), whereas in (b) the spectrum is thresholded at level 57.

TABLE 1. Parameters calculated using the spectral-partitioning algorithm SPA described in section 3 for the trimodal Wavescan spectrum shown in Fig. 1b. Angular values are measured counterclockwise from east.

Row	Region	P	$1/f^{avg}$ (s)	θ^{avg} (°)	$1/f^{max}$ (s)	θ^{max} (°)
1	R	1	10.0	152	12.9	76
2	R_0	0.42	9.7	273	9.4	284
3	R_1	0.58	10.9	100	12.9	76
4	R_{10}	0.40	12.8	79	12.9	76
5	R_{11}	0.18	9.1	120	9.2	120

rameters calculated with the SPA, are given in Table 1. Now $S^l_{R_0}$ is connected for all l, so the algorithm is finished with this region. However, the lowest l such that $S^l_{R_1}$ is not connected is 57, which specifies a fractionation of R_1 into R_{10} and R_{11} according to (4). These regions are shown in Fig. 2b. The values M_{10} and M_{11} are calculated with (5) and give P_{10} and P_{11} using (6). If $S_{R_{10}}$ and $S_{R_{11}}$ specify separate wave systems, then P_{10} and P_{11} can be used to fractionate the variance already attributed to S_{R_1}, namely $V \times P_1$, into two portions: $V \times P_{10}$ and $V \times P_{11}$.

The parameters shown in Table 1 can be arranged in a structure having the shape of a "tree," which for the trimodal Wavescan spectrum is shown in Fig. 3a. The abscissa in this figure is angle θ^{max} (at the top levels) or θ^{avg} (at other levels) from 0° to 360° measured counterclockwise from east. The ordinate is spectral amplitude scaled between 0 and 255. The "tops" of the tree correspond to the three spectral maxima, having normalized amplitudes 255, 164, and 133. The levels at which these treetops join, that is, 57 and 23, are the heights of the spectral saddle points that separate the maxima. It can be seen from this example that the tree structure is natural for the noise reduction operations that follow. The most credible way of computing averaged wave-system statistics is to average over each of the regions R_0, R_{10}, and R_{11} (rows 2, 4, and 5 of Table 1) if there are three wave systems, regions R_0 and R_1 (rows 2 and 3 of Table 1) if there are two wave systems, or region R (row 1 of Table 1) if there is only one wave system. Once the significance of the individual wave systems is known, the appropriate description has already been calculated by the SPA and is obtained simply by selecting the corresponding rows of Table 1. To determine which information should be used to characterize the wave systems, it is necessary to consider neighboring spectra and the spatial and temporal persistence of features of individual trees. This is the task of the pattern-extraction algorithm, PEA.

Figure 4 illustrates the application of the SPA to the Wavescan spectral series over a 5-day interval during LEWEX. Only a subset of the parameters calculated with the SPA is represented in this graph. The modal location estimates and the estimate of the variance attributable to the "wave system" specified by that mode have been used to define a vector, the direction of which encodes the propagation direction defined by the modal estimate. Propagation toward the north is represented as a vector pointing toward the top of the page. The length of this vector has been made proportional to an estimate of the SWH attributable to the wave system it represents. This estimate is obtained from the strength estimates calculated previously, since an estimate of the variance attributable a component wave system is *total wave height variance* $\times P_I$, so that the partitioned significant wave height (PSWH) is *total significant wave height* $\times P_I^{0.5}$. Another descriptive parameter, the logarithm of modal frequency, is displayed as the ordinate in this graph, and time is the abscissa. Comparison of Fig. 1 with Figs. 4 and 5 will illustrate the correspondence between spectra and wave-system–reduced parameters.

Patterns are obvious in Fig. 4; essentially seven subpatterns can be seen, within which the parameters displayed vary continuously. By comparing these patterns to those derived from other data sources, and through a consideration of the meteorological sources, the patterns in Fig. 4 were judged in Gerling (1991) to represent four of the six wave systems that largely explain the LEWEX wave-field variability. For comparison, Fig. 5 gives the corresponding plot for the WAM. For each of the wave systems represented in Figs. 4 and 5, the PSWH, modal period and direction, and average

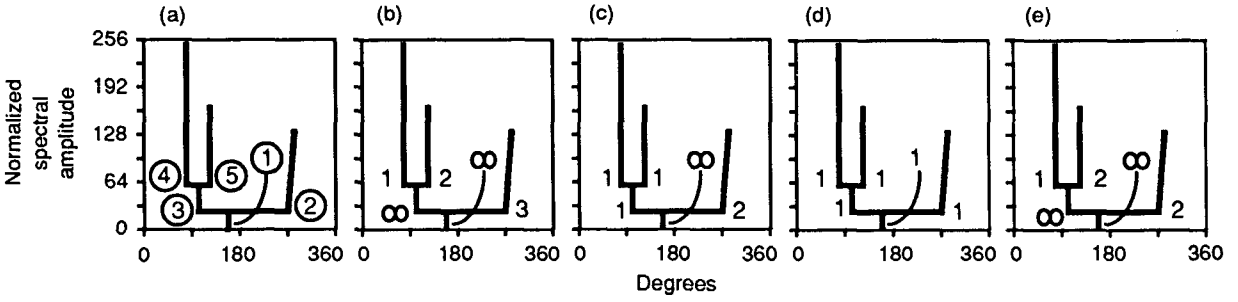

FIG. 3. (a) Schematic representing the hierarchical "tree-shaped" data structure for the trimodal Wavescan spectrum shown in Fig. 1b. Also shown in (b)–(e) are various wave systems that can be parameterized with this structure using the labeling information determined by the PEA.

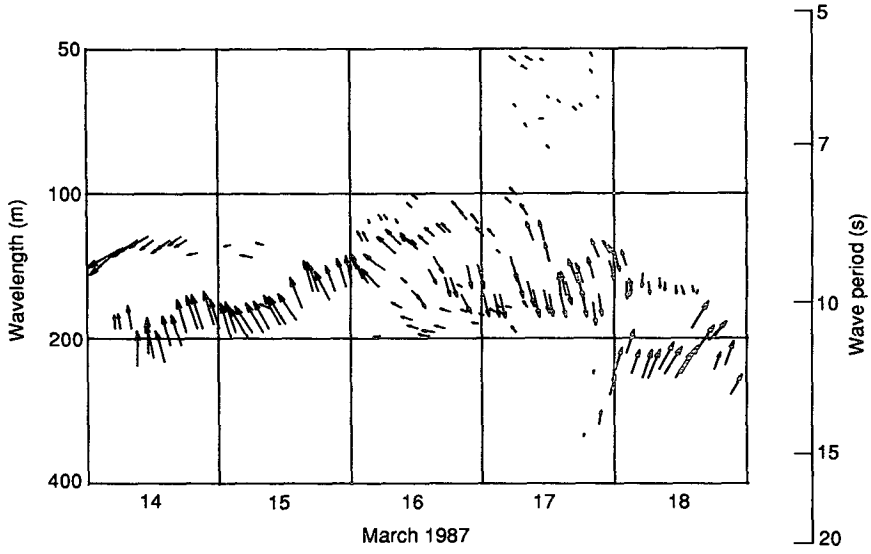

FIG. 4. Vectors representing the time evolution of wave systems observed by the Wavescan buoy at 50°N, 45°W during the LEWEX time period. Partitioned SWH is encoded in length, and the direction indicates wave propagation direction, with north being indicated as toward the top of the page.

period and direction can be parameterized as functions of time. For example, the PSWH of the wave system propagating toward the south-southeast, present after 15 March in Figs. 4 and 5, is given in Fig. 6 for the WAM, VAG, and GSOWM models, as well as for the Wavescan buoy. These curves show very clearly that the major differences among data sources for this southerly propagating system is that the models lead the buoy by perhaps 12–18 h. This type of high-level difference is easily described using the methods discussed in this article but is difficult to obtain otherwise from the original spectra. Moreover, this difference was not evident from examination of either total SWHs or average directions. For other wave-system comparisons and an interpretation of these wave systems in terms of the generating wind systems during LEWEX, see Cardone (1991) and Gerling (1991).

The functioning of the PEA will now be illustrated using the trimodal Wavescan spectrum just discussed. A set of statistics, indicated with numbered circles in

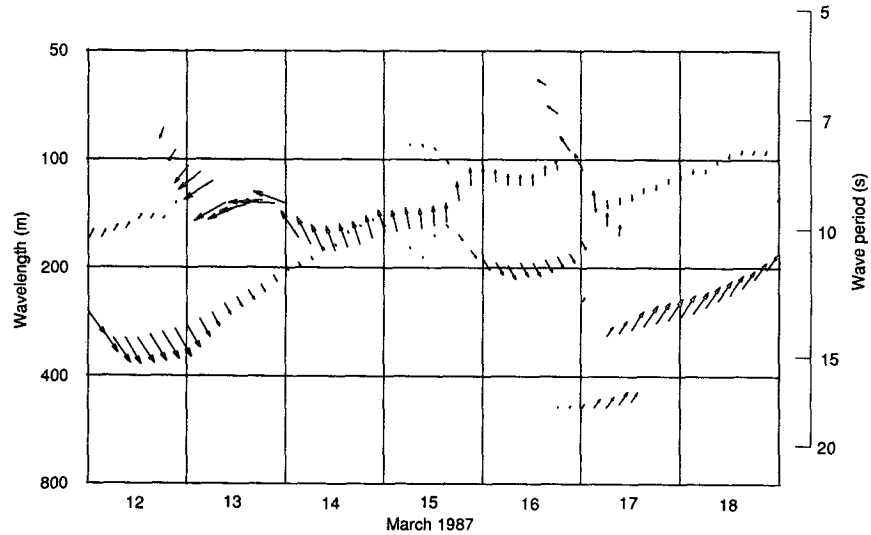

FIG. 5. Vectors representing the time evolution of wave systems predicted by WAM at 50°N, 45°W during the LEWEX time period. Representation is the same as in Fig. 4.

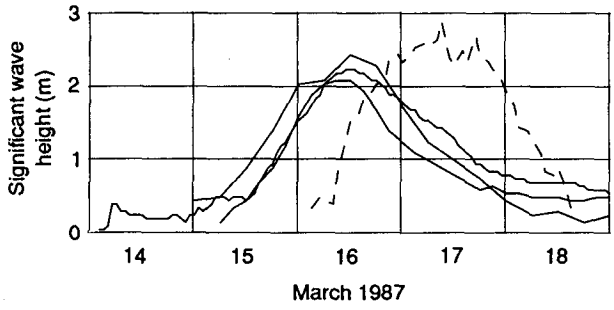

FIG. 6. Partitioned SWH curves for the wave system propagating toward the south-southeast. The WAM, VAG, and GSOWM models are shown with solid lines, and the Wavescan buoy is shown with a broken line.

Fig. 3a, resides at each tree branch node of the data structure describing the spectrum. Each circled number identifies a row in Table 1. Each set of statistics can be represented as a vector $\mathbf{U}_{I,j} = (p_j, l_{I,j}, m_{I,j}, \mathbf{S}_{I,j})$, where the subscript j is an index unique for each spectrum, the subscript I is an index in the hierarchical description of the spectrum, p_j indicates the geographical and temporal position of the spectrum, $l_{I,j}$ is the wave system label,[2] and $m_{I,j}$ is the location of the spectral maximum over the region $R_{I,j}$ and is included to facilitate processing of the tree in a subsequent step. Finally, $\mathbf{S}_{I,j}$ is $(P_{I,j}, f_{I,j}^{\text{avg}}, \theta_{I,j}^{\text{avg}}, f_{I,j}^{\max}, \theta_{I,j}^{\max})$, where each of the variables has already been defined in section 2.

The PEA at present only considers the three parameters $f^{\max}$, $\theta^{\max}$, and P and initially assumes that all maxima potentially represent distinct wave systems. For the Wavescan spectrum parameterized in Table 1, the values contained in rows 2, 4, and 5 are therefore initially used to construct three estimates of S_I. Parameter values from neighboring spectra are compared to determine if the wave systems of one spectrum are contained in the same pattern as the wave systems of another spectrum. If so, they are assigned the same value for a wave system label l:

$$l_{I,m} = l_{J,n} \quad \text{if and only if} \quad d_0(p_m, p_n) \leq T_0 \quad \text{and} \quad d_1(\mathbf{S}_{I,m}, \mathbf{S}_{J,n}) \leq T_1,$$

where d_0 is a metric that specifies the geographical and temporal distance between spectral locations and d_1 is a metric specifying closeness of parameter values. Parameters T_0 and T_1 are threshold values. These metrics and thresholds vary with the application. For example, in the time series of WAM spectra from which Fig. 5 was computed, the interval between estimates is 3 h. In this case, p_m is time measured in hours and T_0 has the value 3. The metric d_1 that has been used in the PEA thus far is simply a "box" metric:

$$d_1(\mathbf{S}_{I,m}, \mathbf{S}_{J,n}) = \begin{cases} 1 & \text{if } 1/t_{10} \leq f_{I,m}^{\max}/f_{J,n}^{\max} \leq t_{10} \\ & \text{and } |\theta_{I,m}^{\max} - \theta_{J,n}^{\max}| \leq t_{11} \\ & \text{and } 1/t_{12} \leq P_{I,m}/P_{J,n} \leq t_{12} \\ 0 & \text{otherwise,} \end{cases}$$

where t_{10}, t_{11}, and t_{12} are three scalar thresholds having typical values of 1.25, 20°, and 8. Logarithms are used to calculate the ratios involved and are calculated initially only once. These distances can therefore be calculated very rapidly.

The PEA presently consists of the automatic portion just described and also a manual portion in which the program functions as a "graphical editor" of the tree structures. It does not appear possible to obtain completely satisfactory wave systems with the simple metrics just defined. The human operator performs final adjustments, such as joining and separating wave systems and removing wave systems considered to represent noise. However, the automatic portion does perform the great majority of the work, and future enhancements will undoubtedly match the operator's intuition more and more closely. Once the wave-system label values l are determined in the PEA for all the treetops, the PA selects the correct level of description for the wave systems. To understand its workings consider Fig. 3 again. Different possibilities for wave system labeling are indicated in Figs. 3b–e. There are at most three possible wave systems, and these are denoted by 1, 2, and 3 located at the appropriate treetops in the diagrams. Figure 3b corresponds to the three wave systems having averaging regions R_0, R_{10}, and R_{11}; Fig. 3c to the two wave systems having averaging regions R_0 and R_1; and Fig. 3d to the situation of having only one wave system. In the latter case, the entire support of the spectrum, R, is used as the averaging region. Figure 3e shows an unlikely grouping in which the maximum at 76° is judged to represent one wave system, and the combination of the modes located at 120° and 284° represents the other. This grouping does not fit the hierarchical model, and special calculations are necessary to compute wave-system statistics.

The tree is processed in two stages. During the first, l is determined at each node of the tree structure, and during the second, a subset $\mathbf{U}_{I_0}, \ldots, \mathbf{U}_{I_n}$ of the statistics describing the n wave systems is formed. As discussed earlier, PEA has set the values of l at treetops to either a group label or a value that does not correspond to any group label and is represented here as ∞. Label values at other nodes are first initialized to zero. Now, beginning at each treetop, proceed "down the tree," setting l_I to the label value residing at the treetop until a nonzero l_I is reached. If that value is different from the one being propagated, then ∞ is propagated down the tree from that point onward. If a treetop is not classified as a wave system initially, then it would be labeled with ∞ and the previously described operation

[2] Hereafter, l denotes the *label* value not the *level* value defined in section 2.

would occur as before. At this point, a list of statistics representative of the wave systems can be constructed. Start again at the treetops that are not labeled with ∞. Continue down the tree until either l_I or m_I changes. If l_I changes, then save the corresponding $\mathbf{U}_I$ in the list. If m_I changes but l_I does not, then this path need not be followed further, since it represents a wave system composed of multiple treetops (in which several spectral maxima are judged to correspond to the same wave system). In this case, only one treetop, that corresponding to the overall maximum of the multiple maxima, is allowed to contribute to the list.

Finally, a set of statistics representative of each wave system determined with the PEA can be obtained from this list. If a particular wave-system label occurs only once in this list, then the statistics $\mathbf{U}_I$ that contain this unique wave-system label can be used to characterize the wave system. This occurs with the examples depicted in Figs. 3b–d. However, in Fig. 3e, which depicts a possible but unrealistic result from the PEA, the list will consist of statistics $\mathbf{U}_{10}$, $\mathbf{U}_{11}$, and $\mathbf{U}_0$. In this case, l_{11} and l_0 both have the value 2, and $\mathbf{U}_{11}$ and $\mathbf{U}_0$ must be combined to give a unique description for the wave system. This is done in the obvious way. This last situation rarely occurs in practice and usually only when one of the modes represents noise.

In the present usage, the SPA, PEA, and PA are done in sequence. The SPA can be done before the other two steps with little loss of information. This is fortunate, since it is a relatively computationally intensive step that requires the full spectrum. It accomplishes a considerable data reduction and delivers statistics that capture a large amount of the spectral information to the subsequent steps in a convenient format. A future, fully automated PEA might really be a combination of the PEA and the PA. Patterns in the SPA parameters obtained with the PEA could be more effectively determined if the correct amount of averaging and noise reduction had already been done. The PEA in this case would determine its groups by selecting from a set of tree nodes that are more representative of real wave systems, rather than from all treetops. This implies a sort of iterative application of PEA and PA, and a working hypothesis is that the SPA calculates information sufficient for this task without feedback information from PEA.

4. Error estimates for the spectral-partitioning algorithm and alternative partitioning algorithms

It would be desirable to have an idea of the errors that can occur using this procedure. However, it is not possible to determine the errors completely since they come from several sources and not all can be precisely characterized. Two of these sources are statistical variability and variability due to the choice of partitioning algorithm. Different procedures are needed to characterize the statistical variability in model spectra verses buoy spectra. The ultimate source of model spectral variability is uncertainty in the wind field (although the issue could be further complicated by considering differences in model physics). If wind-field errors are known, their effect on spectra can be determined through analysis of multiple model runs, each using a different realization of the wind field. This procedure is time-consuming and nonstandard, however. Cardone (1991) discusses the effect of two different LEWEX hindcast wind fields on the ODGP model spectra. The difference between the two wind fields used in that study indicates the possible error in these estimates that were determined from sparse observations.

For buoy spectra, a standard statistical spectral variability occurs because of the finite length of the time series of heave and east and north slope. However, MEM is highly nonlinear, and probably the only reliable way of determining the effect of this variability on directional spectral estimates is through Monte Carlo simulations. A more accessible "estimate" can be obtained for some wave systems over some time periods simply by inspection of the vector plots. For example, consider the peak frequency and direction of the dominant wave system from 1200 UTC 14 March through 1200 UTC 16 March in the Wavescan plot shown in Fig. 4. One could assume that the slow variation represents true wave variability and the residual represents statistical error. Another element of the buoy spectral variability is that due to the particular spectral reconstruction method used, but this will not be addressed in this article.

The variability due to partitioning method will be discussed by showing results obtained with several plausible alternative partitioning methods on a sequence of VAG spectra. Algorithms implementing these alternatives have not been constructed; the results discussed here have been obtained through a laborious examination of individual spectra.

Figure 7 gives a sequence of 24 VAG spectra from LEWEX at the *Tydeman* location (50°N, 45°W) from the period 0000 UTC 12 March through 2100 UTC 14 March. The spectra of this series will be used to illustrate the application of various partitioning methods and also the effect of the discrete nature of the spectra on the calculations. Evident in this series is a diminishing swell from the northwest (the Labrador Sea) and a growing wind sea initially from the northeast that evolves with a changing wind to finally be from the southeast. First consider the spectrum occurring at 0000 UTC 13 March. The numerical values for a portion of the frequency spectrum ($m^2\ s^2$) normalized to have a maximum value of 255 are given in Table 2. On this scale, 51 is the level [identified as l_0 in (1)] at which the spectral masses corresponding to these two systems, the swell from the northwest and the evolving wind sea, separate in the thresholded spectrum. Another local maximum having value 159 is present in Table 2, but it is considered to be part of the wave

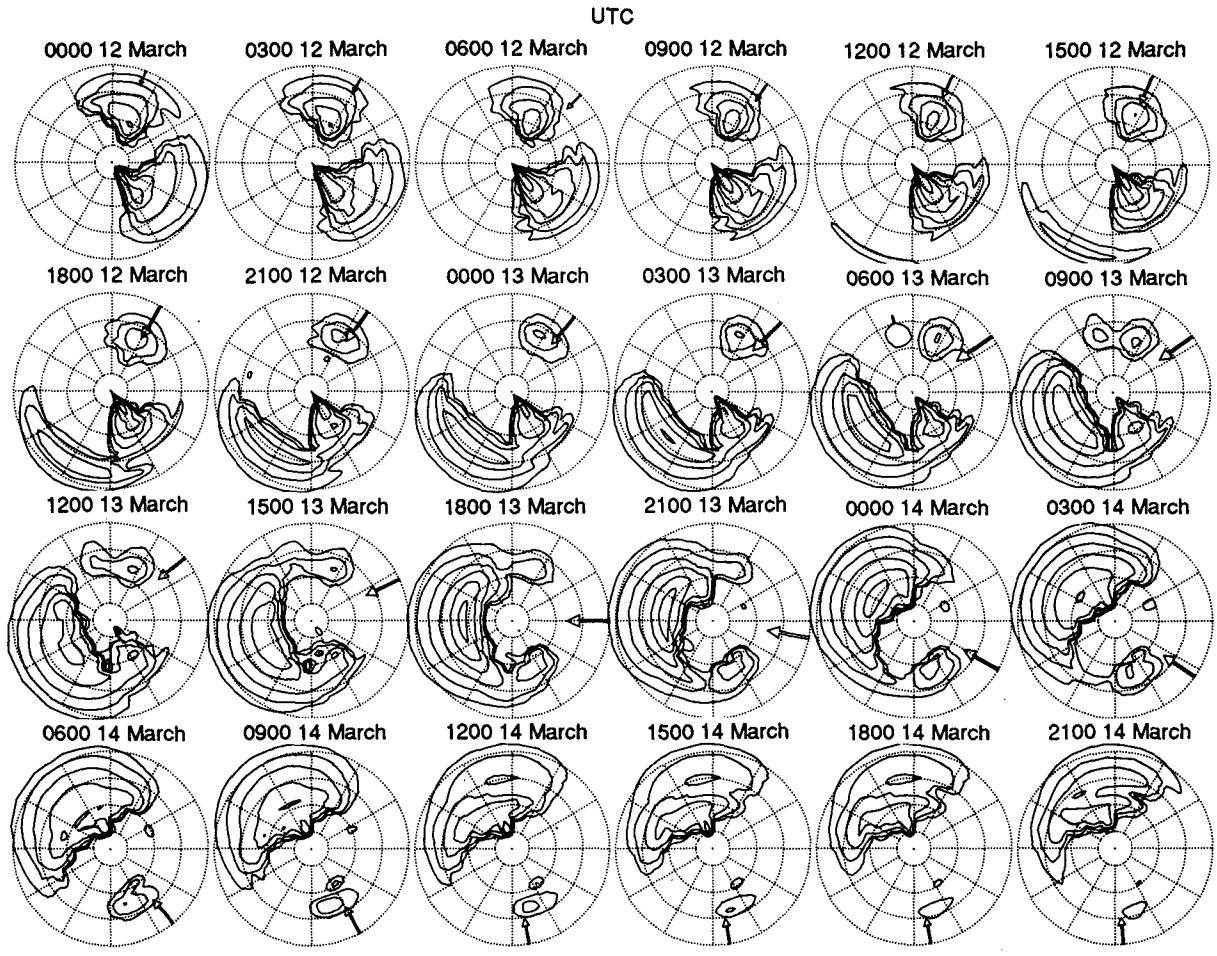

FIG. 7. Sequence of directional spectra predicted by the VAG model at 50°N, 45°W during the LEWEX time period from 0000 UTC 12 March through 2100 UTC 14 March 1987. Arrows represent wind propagation direction and speed. Each frequency calibration circle represents a wind-speed increment of 10 m s^{-1}.

system represented by the value 255. It is apparent from this example that the convention to join regions connected only along a diagonal path is being used; otherwise, l_0 would have the value 50. This is analogous to the choice that must be made in contouring programs; whether to construct more "hills" or more "valleys." Since "hills" can be connected along a diagonal path, "valleys" by necessity cannot. This convention was chosen since a spectral peak might manifest itself with only one element in certain noisy spectra, and implies, in effect, that such a weak signature does not constitute a wave system. In Fig. 7, a weak swell from the southwest is also evident but is not represented in the tabular values. As can be seen in Table 2, 10 elements are contained in the lower-frequency swell region R_0 and 11 elements are contained in the wind-sea region R_1. The weights for partitioning the total variance between the two wave systems calculated with (3) using these regions are 0.36 and 0.64.

Another partitioning algorithm could be constructed that would use all spectral values in its computation rather than the values that exceed a particular level. Starting at spectral saddle points, proceed along the path of steepest descent to partition the spectrum into regions belonging to one wave system or the other. An example of how this algorithm would work on our test spectrum is given in Table 3. Indicated there are the two averaging regions corresponding to the wind sea and swell, the saddle point (value 50), and the path of steepest descent that separates the regions. The saddle point and the path were determined visually. Although it might be difficult for the reader to see this saddle point in the tabular values, its existence is guaranteed by consideration of the behavior of level curves in the vicinity. The weights P_0 and P_1 calculated with these regions are 0.25 and 0.75. Constructing an algorithm to determine the path automatically would be more difficult than constructing the algorithm described in this paper. In fact, it would probably use the SPA as a starting point, since the levels and regions specified in (1), (4), and (7) could be used to locate saddle points. This procedure has been applied to the 3-day series of

TABLE 2. Numerical values for a portion of the VAG wave spectrum (units of $m^2 s^2$) occurring 0000 UTC 13 March 1987 at 50°N, 45°W. The spectrum has been normalized to lie within the range of 1-byte integers 0–255. The swell region R_0 contains the maximal value 255, whereas the wind-sea region R_1 contains the maximal value 131. Both regions are identified with boldface numerals.

f (Hz)	θ (clockwise from north)											
	85°	105°	125°	145°	165°	185°	205°	225°	245°	265°	285°	305°
0.05	0	0	0	11	0	0	0	0	0	0	0	0
0.06	0	0	0	**114**	0	0	0	0	0	0	0	0
0.06	0	0	2	**255**	29	0	0	0	0	0	0	0
0.07	0	3	0	**222**	**77**	0	0	0	0	0	0	0
0.08	0	0	0	**134**	**109**	0	0	0	0	0	0	0
0.09	0	0	14	**159**	**102**	0	0	0	0	0	0	0
0.09	0	5	33	**107**	**74**	0	23	25	8	0	0	0
0.10	0	6	10	25	50	20	48	**51**	42	0	4	0
0.11	0	0	24	21	24	**72**	**101**	**107**	**89**	18	9	0
0.13	2	4	7	6	18	**88**	**123**	**131**	**108**	**66**	8	0
0.14	0	7	0	4	19	36	50	**53**	44	26	3	0
0.15	0	6	0	2	9	19	27	29	24	14	4	0
0.17	0	0	0	0	6	13	18	19	16	9	2	0
0.18	0	0	0	0	4	8	11	12	10	6	0	0
0.20	0	0	0	0	2	5	7	7	6	3	0	0
0.22	0	0	0	0	0	3	4	4	3	2	0	0
0.25	0	0	0	0	0	0	2	2	2	0	0	0

VAG spectra surrounding this particular spectrum. The PSWH curves for the two wave systems under consideration are shown in Fig. 8. Shown there are curves for both SPA from 0000 UTC 12 March through 0000 UTC 17 March and also for the saddle-point algorithm from 0000 UTC 12 March through 2300 UTC 14 March. The monotonically decreasing curves correspond to the diminishing swell from the northwest, whereas the other curves represent the wind sea that exceeds 5 m on 14 March. As can be seen, the differences apparent at 0000 UTC 13 March between the two methods are nearly the largest that occur over the range examined, and only minor differences occur elsewhere.

Another possibility for the partitioning algorithm collapses the two-dimensional spectrum along one dimension and partitions the resulting one-dimensional spectrum at local minima. This calculation has been applied to our test spectrum collapsed along the frequency dimension. In this case, the angular cross section spanning 105°–165° was used as R_0 and that spanning 185°–285° was used as R_1 in (2), giving values of 0.30 and 0.70 for the partitioning weights. This does not represent a general method, however, since

TABLE 3. Numerical values for the same spectrum shown in Table 2 illustrating the partitioning resulting from the saddle-point method. The value 50 is the saddle point, and the partitioning proceeds down the path of steepest descent.

f (Hz)	θ (clockwise from north)											
	85°	105°	125°	145°	165°	185°	205°	225°	245°	265°	285°	305°
0.05	0	0	0	**11**	0	0	0	0	0	0	0	0
0.06	0	0	0	**114**	0	0	0	0	0	0	0	0
0.06	0	0	**2**	**255**	**29**	0	0	0	0	0	0	0
0.07	0	**3**	0	**222**	**77**	0	0	0	0	0	0	0
0.08	0	0	0	**134**	**109**	0	0	0	0	0	0	0
0.09	0	0	**14**	**159**	**102**	0	0	0	0	0	0	0
0.09	0	**5**	**33**	**107**	**74**	0	**23**	**25**	**8**	0	0	0
0.10	0	**6**	**10**	**25**	**50**	**20**	**48**	**51**	**42**	0	**4**	0
0.11	0	0	**24**	**21**	**24**	**72**	**101**	**107**	**89**	**18**	**9**	0
0.13	2	**4**	**7**	**6**	**18**	**88**	**123**	**131**	**108**	**66**	**8**	0
0.14	0	**7**	0	**4**	**19**	**36**	**50**	**53**	**44**	**26**	**3**	0
0.15	0	**6**	0	**2**	**9**	**19**	**27**	**29**	**24**	**14**	**4**	0
0.17	0	0	0	0	**6**	**13**	**18**	**19**	**16**	**9**	**2**	0
0.18	0	0	0	0	**4**	**8**	**11**	**12**	**10**	**6**	0	0
0.20	0	0	0	0	**2**	**5**	**7**	**7**	**6**	**3**	0	0
0.22	0	0	0	0	0	**3**	**4**	**4**	**3**	**2**	0	0
0.25	0	0	0	0	0	0	**2**	**2**	**2**	0	0	0

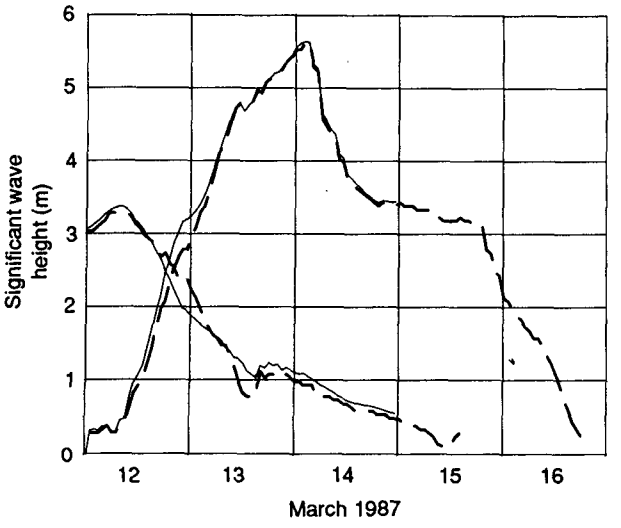

FIG. 8. Partitioned SWH for the swell and wind-sea wave systems predicted by the VAG model at 50°N, 45°W during the LEWEX time period. Values calculated by SPA are connected by a thick broken line, whereas those calculated by the saddle-point method are connected by a thin solid line. The latter values were only calculated for the time period 0000 UTC 12 March through 2300 UTC 14 March 1987.

resolution is lost by collapsing one dimension. For example, if two systems occur at the same frequency, then they will not be resolved in the one-dimensional frequency spectrum. It will therefore be impossible, in general, to associate a variance estimate obtained in this way with each modal location of the directional spectrum. Other possibilities for partitioning algorithms include the application of the SPA to some transformation of the spectrum; for example, integrated spectral elements. In this case, the array with elements proportional to $S(f_i, \theta_j)$ shown in Table 2 would be replaced by one whose elements are proportional to $S(f_i, \theta_j)\Delta f_i \Delta\theta_j$. The effect of using integrated values is to increase the effect of the higher frequencies. Indeed, R_0 now consists of 8 elements, whereas R_1 contains 17. The use of these new regions in (3) gives the partitioning weights 0.28 and 0.72. Finally, another possibility would partition the spectral support according to a Dirichlet tessellation (Ripley 1981) constructed using the set of local spectral maxima. The principal advantage of this method is that it is relatively easy to implement, although the resulting algorithm is probably not faster than the SPA, since it requires calculating many distances. However, it is easy to construct test spectra that result in an obviously incorrect partitioning of the spectral region of support among the component wave systems. The SPA, since it uses information that is more directly related to spectral energy, namely, the complete set of spectral amplitudes, is likely to provide more believable estimates of wave system energy.

The SPA is more prone to error the more that wave systems overlap. The spectra in Fig. 7 show an interesting situation in which two wave systems that are initially quite separate further overlap and finally begin to separate again. This occurs as the northwesterly swell system evolves toward higher frequencies and the wind sea grows with constant wind. The separation near the end of the sequence occurs as the wind changes direction, commencing at about 1400 UTC 13 March. Continuity in PSWH can be expected, considering the continuity of the spectra and wind. However, a slight decrease in PSWH as calculated with SPA is apparent in Fig. 8 from 1200 UTC through 1500 UTC 13 March. This decrease can be explained through consideration of the size of the averaging region for the swell system, R_0. From 0000 UTC through 0800 UTC 13 March, nine elements are in the averaging region, but from 1200 UTC through 1500 UTC, only two elements are in R_0. After that time, the number increases again to five. The curve in Fig. 8 representing PSWH calculated with the saddle point method does not show the decrease from 1200 UTC through 1500 UTC, which further confirms that the decrease is an artifact resulting from the large degree of overlap between the two regions. However, the presence of a slight increase at 1500 UTC also shows that obtaining completely smooth curves with any algorithm is not easy.

Another potential problem is illustrated with the spectral sequence of Fig. 9, which shows a series of three WAM spectra from 0600 UTC through 1200 UTC 17 March. An easterly wind sea gradually becomes southerly, and at 1200 UTC, a swell system from the southwest merges with the wind sea. Even though the spectrum at 1200 UTC differs very little from that at 0900 UTC, the two wave systems that were separated at 0600 and 0900 UTC are represented as one from 1200 UTC onward because the system from the south-southeast no longer manifests a separate peak.

The utility of the tree structures in producing wave system parameter estimates having the appropriate degree of averaging can be seen by consideration of the

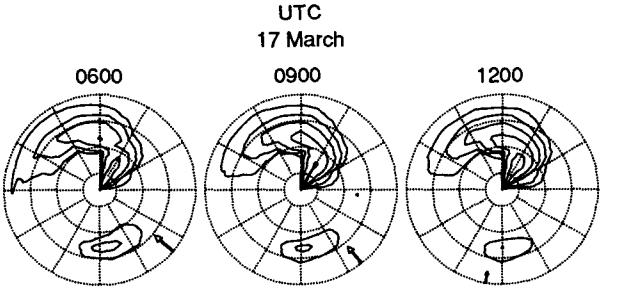

FIG. 9. Sequence of three WAM spectra. The north-northwesterly propagating system is present only through 0900 UTC 17 March in the vector diagram of Fig. 5. However, the spectral variance in this portion of the spectrum remains undiminished for another 6 h.

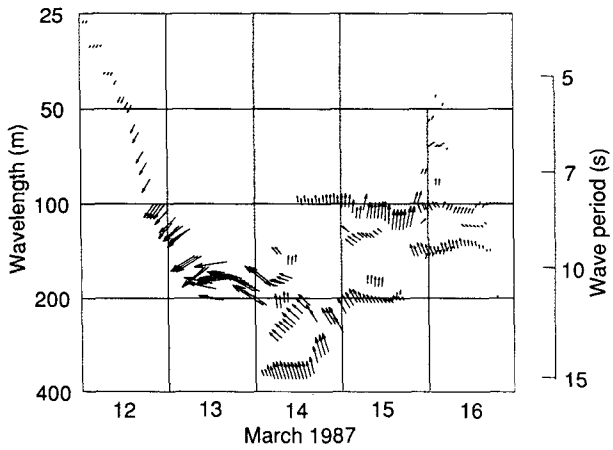

FIG. 10. Vector plot for the wave system aligned with the local wind direction that was predicted by the VAG model at 50°N, 45°W during the LEWEX time period. The format is similar to that of Figs. 4 and 5.

vector plot shown in Fig. 10 for the VAG wave system just discussed that was aligned with the local wind. In contrast to the multimodal signature exhibited by VAG, WAM and Wavescan both showed essentially a unimodal distribution for this wave system (see Figs. 4 and 5). The probable cause of this difference was discussed in Gerling (1991) and involves the separate treatment of wind sea and swell by VAG and many other second-generation models [see the report by The SWAMP Group (1985)]. Over the spectral region determined to be wind sea, the spectrum is constrained to be parameterized, a Joint North Sea Wave Project (JONSWAP) spectrum (Hasselmann et al. 1973), for example, whereas over the rest of the spectrum, the discrete spectral components might propagate independently. Nonlinear transfers are less general than in third-generation models, and are specified in terms of reduced parameters, such as those of JONSWAP. Since the region over which the wave spectrum is considered to be wind sea varies with wind speed and direction, models such as VAG generally exhibit more spectral modes than either first- or third-generation models, although they may agree well in integrated parameters such as total SWH or component wave system PSWH. The PSWH curve corresponding to Fig. 10 is the curve in Fig. 8 that exceeds 5 m in SWH. To determine this curve, intermediate nodes in the tree structures describing the VAG spectra were selected by the methods described previously. This VAG-determined PSWH curve agreed with the corresponding Wavescan curve (not shown) better than any other model discussed in Gerling (1991).

5. Application to fields of spectra

The major advantage in using a data reduction method such as that described in this paper is realized when considering large datasets. For only a few spectra, there is little need for reduced parameters, but for very large datasets, such as those presently generated by operational numerical wave models and anticipated from future satellite remote sensing systems, there is a need for a data-reduction method that preserves directional information in a meaningful way.

Figure 11a displays the average wave directions for GSOWM over the North Atlantic at 0000 UTC 16 March 1987. Total SWH is encoded in vector length, and direction indicates the direction toward which waves propagate. The field contains a clockwise wave circulation pattern centered at 50°N, 20°W, and two counterclockwise patterns farther south. The low at 38°N, 55°W generated waves in excess of 10 m in SWH. Also apparent is a "shearing" in the wave pattern at 45°W between 48° and 55°N. At this location, a 180° shift in average wave direction occurs at adjacent grid points.

The component wave systems give a somewhat different picture of the variability present in the wave field. These are illustrated in Fig. 11b. This is a rather confusing pattern of overlapping wave systems, so each system is shown separately in Figs. 12a–d. These wave systems were determined essentially by the automatic portion of the PEA, with very little intervention by the operator. The wave system in Fig. 12a accounts for 60% of the amount of total wave height variation over that region, whereas those in Figs. 12b–d account for 18%, 11%, and 6%, respectively. In all, these four wave systems account for 95% of the total wave height variation in the region shown, and the portion not accounted for was primarily small-scale, coastal activity. The shearing in the wave pattern of Fig. 11a is not present in any of the component wave systems. These vary continuously, except in the region of high waves near 40°N, 55°W, where rapid spectral variation occurs and partitioning among the three contributory wave systems is not easy. The wave system depicted in Fig. 12c is also probably too complex to be considered a single system. Enhancements to the PEA could result in the cleavage of this system into three component systems, each of which would present a more uniform variation in direction and partitioned SWH. This is, however, a straightforward task to accomplish with the manual portion of the PEA. The wave systems shown in Figs. 12b–d all contribute to the shear flow pattern at 45°W commented on previously. This pattern is seen to be the result of the summation of two opposing wave systems in the average wave-direction computation. The resulting average direction is, in this case, simply the direction of the more energetic wave system. The southeasterly wave system of Fig. 12b does not appear to influence the average direction in the shear region, even though it is a significant component of the wave field variability in that region. Also apparent from the partitioned wave systems is that the clockwise

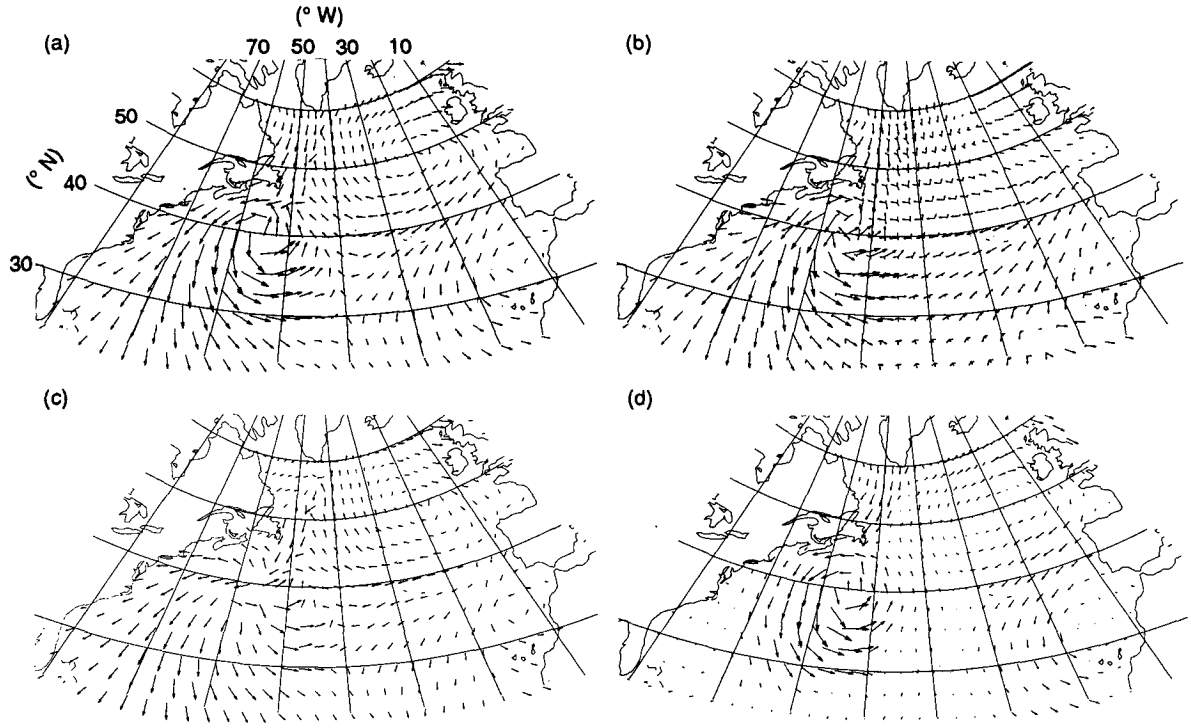

FIG. 11. Wave fields generated by the GSOWM model at 0000 UTC 16 March 1987: (a) average wave direction, (b) partitioned wave-system directions overlaid, (c) swell field, (d) wind sea.

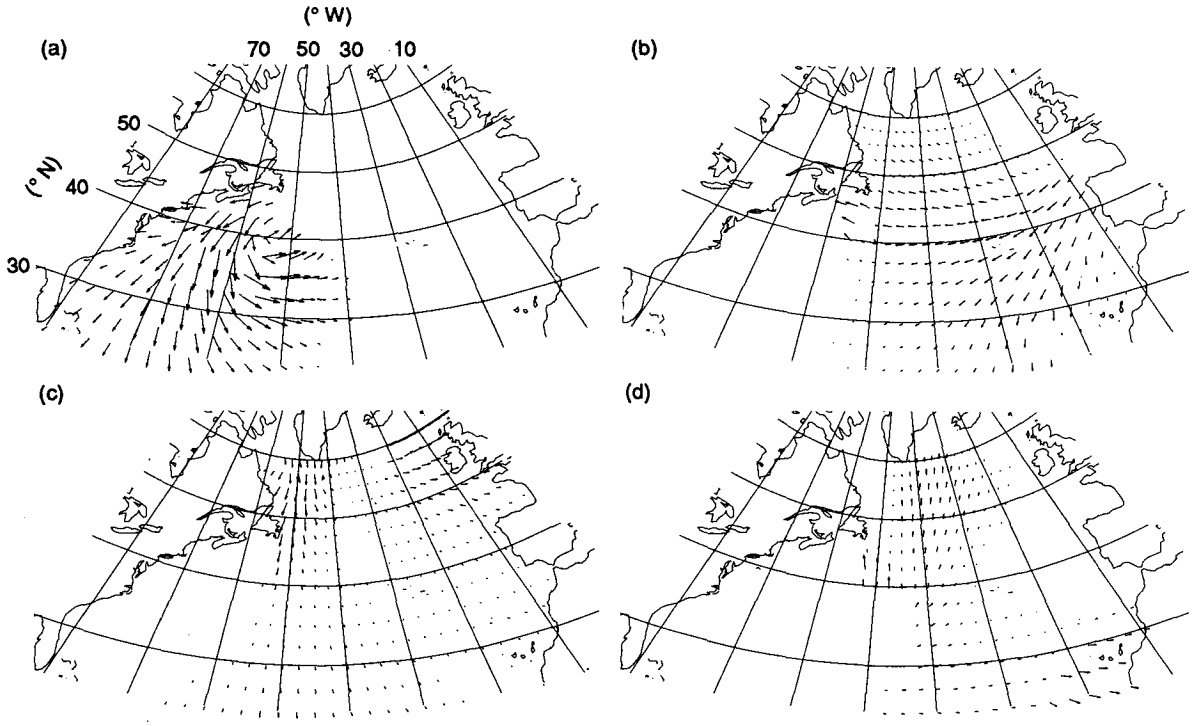

FIG. 12. Partitioned wave systems shown in Fig. 11b, separated and ordered from most energetic (a) to least energetic (d).

circulation pattern in the average directions of Fig. 11a centered at 50°N, 20°W is misleading. A more accurate description is given in Fig. 12, where it is seen that the circulation is really the average of the three component wave systems, all of which are fairly uniform in direction over that region.

Also shown are the swell (Fig. 11c) and wind sea (Fig. 11d) for the wave field. The wind sea was defined in the same way as it was by The WAMDI Group (1988), namely, as "that part of the spectrum for which the component of the friction velocity u_* in the direction of wave propagation is greater than 0.05 times the wave phase velocity (corresponding approximately to $U > 1.2c$)." The remaining spectrum defines the swell. The directions of the wind sea are actually quite close to the directions of the wind itself (not shown). The wind sea-swell decomposition is not as informative as that shown in Fig. 12.

6. Summary

This article has discussed a new method for the analysis of directional wave spectral data. It is general in that it does not make assumptions regarding spectral form, and it can be applied to directional spectral estimates from any source, including numerical wave model spectra, radar image spectra, and directional wave buoys. The method consists of three stages. The first is a data-intensive stage, called SPA, in which spectra are reduced to tree-shaped data structures that are claimed to be sufficient for the stages that follow. The next stage, called the PEA, characterizes large-scale spatial and temporal patterns in the parameters previously extracted and identifies them as "wave systems." The third stage, as presently implemented, reprocesses the tree structures using the wave system information to provide statistics representing the appropriate amount of averaging. This methodology results in a high-level description of the wave field that is more easily interpretable than parameters such as average direction and total SWH or wind sea-swell separations. Each of the resulting wave systems is normally the result of a meteorologically distinct event.

The spectral-partitioning method assumes that each spectral mode potentially represents a distinct wave system. An estimate of the SWH attributable to that wave system is computed in a manner analogous to the computation of conditional probabilities. The scheme is nonparametric and has produced reasonable estimates of wave system parameters for all spectra to which it has been applied. This is a distinct advantage over a least-squares approach that might attempt to represent a general wave spectrum as a superposition of parametric forms, each of which would represent a separate wave system. Such a scheme would likely be confounded by some "abnormal" spectrum that would result in unreasonable values.

No significant deficiencies have been found in the spectral-partitioning algorithm. An arguably more correct procedure that uses the entire spectrum for its calculations rather than thresholded spectra was applied to a spectral series but exhibited only minor differences from the SPA. Possibly the main disadvantage of the SPA is the requirement that a wave system manifest itself with a spectral mode. More work is needed to produce a fully automatic pattern extraction algorithm. The present algorithm is quite primitive but works surprisingly well. However, the algorithm becomes increasingly unwieldy when applied to larger datasets. For example, to obtain a series of partitioned wave fields over the North Atlantic for GSOWM (one of which is shown in Fig. 12), the operator was required to impose a temporal consistency in the wave systems that were automatically determined for each time. It should be possible to implement this temporal consistency requirement in the PEA also, and work is in progress toward that goal.

This methodology should be useful for wave spectral-comparison experiments similar to LEWEX, which was discussed in this article. It should also be useful for routine processing of wave model analyses, once the pattern extraction algorithm is made sufficiently automatic. Finally, it might be useful for schemes that assimilate spaceborne synthetic aperature radar (SAR) wave spectral estimates into numerical wave models. At present, SAR estimates are of somewhat low fidelity, and parameters such as those extracted by the SPA might even represent the limit of the information present in SAR wave spectral estimates. This information could be highly useful for correcting wind fields, however, since each wave system contains information about its source winds. Moreover, the wave systems extracted by the PEA represent a large data reduction, and they might be computationally easier to assimilate than the complete wave spectrum.

Acknowledgments. The author acknowledges all of the participants in LEWEX (the experiment that motivated this work): in particular, Robert Beal, who coordinated LEWEX; Liana Zambresky and Anne Guillaume, who provided the WAM and VAG spectral series; Paul Wittmann, who provided the GSOWM global spectral dataset; and finally Harold Krogstad who provided the Wavescan data. Discussions with the LEWEX group and also with members of the WAMDI group have been both helpful and enjoyable.

REFERENCES

Allender, J., T. Audunson, S. F. Barstow, S. Bjerken, H. Krogstad, P. Steinbakke, L. Vartdal, L. Borgman, and C. Graham, 1989: The Wadic project: A comprehensive field evaluation of directional wave instrumentation. *Ocean Eng.*, **16**, 505–536.

Audunson, T., S. F. Barstow, and H. E. Krogstad, 1982: Analysis of wave directionality from a heave pitch and roll buoy operated offshore Norway. *Ocean Sci. Eng.*, **7**, 291–319.

Beal, R. C., 1991: *Directional Ocean Wave Spectra.* The Johns Hopkins University Press.

Cardone, V., 1991: The LEWEX common wind field. *Directional Ocean Wave Spectra,* R. C. Beal, Ed., The Johns Hopkins University Press.

Clancy, R. M., J. E. Kaitala, and L. F. Zambresky, 1986: The Fleet Numerical Oceanography Center global spectral ocean wave model. *Bull. Amer. Meteor. Soc.,* **67,** 498–512.

Gerling, T. W., 1991: A comparative anatomy of the LEWEX wave systems. *Directional Ocean Wave Spectra,* R. C. Beal, Ed., The Johns Hopkins University Press.

——, and R. C. Beal, 1991: A SIR-C southern oceans waves experiment. *Oceans from Space—1990,* J. Gower, Ed.

Guillaume, A., 1987: VAG-Modèle de prévision de l'état de la mer en eau profonde. Note de travail de l'Etablissement d'Etudes et Reserches Météorologiques, No. 178. [Available from Service Central D'Exploitation de la Meteorlogie, 2, Avenue Rapp—75340 Paris Cedex 07.]

——, 1990: Statistical tests for the comparison of surface gravity wave spectra with application to model validation. *J. Atmos. Oceanic Technol.,* **7,** 551–567.

——, 1991: Results obtained with the wave model VAG during LEWEX. *Directional Ocean Wave Spectra* R. C. Beal, Ed., The Johns Hopkins University Press.

Hasselmann, K., T. P. Barnett, E. Bouws, H. Carlson, D. E. Cartwright, K. Enke, J. A. Ewing, H. Gienapp, D. E. Hasselmann, P. Krusemann, A. Meerburg, P. Müller, D. J. Olbers, K. Richter, W. Sell, and H. Walden, 1973: Measurements of wind-wave growth and swell decay during the Joint North Sea Wave Project (Jonswap). *Dtsch. Hydrogr. Z., suppl. A.,* **8.**

Krogstad, 1987: Wave data collected by Wavescan during the Labrador Sea Extreme Waves Experiment (LEWEX). Oceanographic Center Report No. 02.0810.00/01/87, [Available from SINTEF Group, N-7034 Trondheim-NTH, Norway.]

Kuik, A. J., G. Ph. van Vledder, and L. H. Holthuijsen, 1988: A method for the routine analysis of pitch-and-roll buoy wave data. *J. Phys. Oceanogr.,* **18,** 1020–1034.

Long, R. B., and K. Hasselmann, 1979: A variational technique for extracting directional spectra from multicomponent wave data. *J. Phys. Oceanogr.,* **9,** 373–381.

Longuet-Higgins, M. S., D. E. Cartwright, and N. D. Smith, 1963: Observations of the directional spectrum of sea waves using the motions of a floating buoy. *Ocean Wave Spectra,* Prentice-Hall, 111–136.

Lygre, A., and H. E. Krogstad, 1986: Maximum entropy estimation of the direction distribution in ocean wave spectra. *J. Phys. Oceanogr.,* **16,** 2052–2059.

Oltman-Shay, J., and R. T. Guza, 1984: A data-adaptive ocean wave directional-spectrum estimator for pitch and roll type measurements. *J. Phys. Oceanogr.,* **14,** 1800–1810.

Ripley, B. D., 1981: *Spatial Statistics.* John Wiley & Sons.

Snodgrass, F. E., G. W. Groves, K. F. Hasselmann, G. R. Miller, W. H. Munk, and W. H. Powers, 1966: Propagation of ocean swell across the Pacific. *Philo. Trans. Roy. Soc. London, A,* **259,** 431–497.

The WAMDI Group, 1988: The WAM model—A third-generation ocean wave prediction model. *J. Phys. Oceanogr.,* **18,** 1775–1810.